Journal of
Applied Remote Sensing

Combining land surface temperature and shortwave infrared reflectance for early detection of mountain pine beetle infestations in western Canada

Michael Sprintsin
Jing M. Chen
Peter Czurylowicz

SPIE

Combining land surface temperature and shortwave infrared reflectance for early detection of mountain pine beetle infestations in western Canada

Michael Sprintsin, Jing M. Chen, and Peter Czurylowicz
University of Toronto, Department of Geography and Program in Planning,
100 St. George Street, Toronto, Ontario, Canada M5S 3G3.
michaelsp@volcani.agri.gov.il; chenj@geog.utoronto.ca; p.czurylowicz@utoronto.ca

Abstract. The current mountain pine beetle (*Dendroctonus ponderosae* Hopkins) outbreak, which began in 1999, continues to be the leading cause of pine tree mortality in British Columbia. Information regarding the location and spatial extent of the current attack is required for mitigating practices and forest inventory updates. This information is available from spaceborne observations. Unfortunately, the monitoring of the mountain pine beetle outbreak using remote sensing is usually limited to the visible stage at which the expansion of the attack beyond its initial hosts is unpreventable. The disruption of the sap flow caused by a blue-staining fungi carried by the beetles leads to: 1. a decrease in the amount of liquid water stored in the canopy, 2. an increase in canopy temperature, and 3. an increase in shortwave infrared reflectance shortly after the infestation. As such, the potential for early beetle detection utilizing thermal remote sensing is possible. Here we present a first attempt to detect a mountain pine beetle attack at its earliest stage (green attack stage when the foliage remains visibly green after the attack) using the temperature condition index (TCI) derived from Landsat ETM+ imagery over an affected area in British Columbia. The lack of detailed ground survey data of actual green attack areas limits the accuracy of this research. Regardless, our results show that TCI has the ability to differentiate between affected and unaffected areas in the green attack stage, and thus it provides information on the possible epicenters of the attack and on the spatial extent of the outbreak at later stages (red attack and gray attack). Furthermore, we also developed a moisture condition index (MCI) using both shortwave infrared and thermal infrared measurements. The MCI index is shown to be more effective than TCI in detecting the green attack stage and provides a more accurate picture of beetle spread patterns. [DOI: 10.1117/1.3662866]

Keywords: mountain pine beetle; water stress; monitoring; thermal infrared remote sensing.

Paper 10188RRR received Nov. 30, 2010; revised manuscript received Oct. 19, 2011; accepted for publication Nov. 1, 2011; published online Nov. 28, 2011.

1 Introduction

Since 1999, the mountain pine beetle (*Dendroctonus ponderosae* Hopkins*)* has affected more than 13 million ha of pine forest in western Canada,[1] causing extensive mortality of its preferred host trees (lodgepole pine, *Pinus contorta Dougl. ex Loud.* var. *latifolia Engelm.*), resulting in a significant ecological change at the landscape level.[2] The current outbreak in British Columbia (BC) has reached epidemic levels, causing serious (∼46%) cumulative volume losses of all merchantable pine stands in the province.[3] The rapid expansion of mountain pine beetle populations can be attributed to the abundance of mature and over-mature lodgepole pine and to several years of favorable climatic conditions, particularly increasing winter minimum temperatures.[4,5]

1931-3195/2011/$25.00 © 2011 SPIE

The phenology of the mountain pine beetle and the associated host response are described elsewhere.[2,6–8] Generally, the interaction between the beetle and the host trees can be divided into three stages:

1. The green attack (GA) stage, which is the period immediately following a successful beetle attack, but before symptoms of the attack (i.e., color change) are visibly evident in the crown.[8,9] The main characteristic of a GA is a drop in sapwood moisture of visibly unchanged trees.
2. The red attack (RA) stage that usually develops within 1 year after GA. During the RA stage, the tree canopy gradually turns yellow and then red-brown.[10]
3. The last stage is called gray attack. This is the period when the needles drop down from the tree following the desiccation of the leaves and the breakdown of the pigment molecules.[11,12]

The mountain pine beetle attack begins in August when adult beetles attack trees and lay their eggs in the phloem tissue beneath the bark. About 2 weeks later beetles hatch as white larvae and aggressively feed on the tree soft tissue over the winter months resulting in host tree mortality. The pupal stage usually ends in late spring, and from mid-July to mid-August, the beetles leave their tunnels and fly to new trees, utilizing the prevailing wind patterns. Approximately 4 to 8 weeks after the attack a decrease in sapwood moisture of up to 50% has been reported.[13] Visible symptoms of an attack are evident in the crown during late May to early June in the year following the initial attack. In rare cases, particularly during unseasonably warm late summer months, the symptoms become visible during the autumn of the attack year.[9] This is also the period when the sapwood moisture decreases further to less than 30% to 35% of the preattack value and the first symptoms of fading become visible. The eggs that were laid in August develop into mature adults approximately 1 year later. Thus, typically within a year of the original (i.e., GA) attack, the trees enter the RA stage that may last for several years until the needles shed from the dead trees.

Information regarding the location of the affected areas and spatial extent of beetle attack is required for mitigating practices and forest inventory updates. Obtaining this information, however, is not straightforward because as it was shown in earlier work the distribution of an MPB attack is governed by the behavioral responses of the attacking beetles to insect- and host-produced odors, light intensity, temperature, humidity, gravitational force, and the surface structure of the bark.[14] Consequently, infection tends to occur in small, dispersed patches[7] that cannot be easily detected by ground surveys.

Since the structures of leaf tissues and leaf (and canopy) moisture content have characteristic patterns of absorption and reflection of electromagnetic energy, the synoptic observations provided by remote sensing could be an ultimate solution for decision making at the landscape level. Unfortunately, the employment of remote sensing techniques for monitoring the effect of the mountain pine beetle is usually limited to the visible (i.e., RA) stage (e.g., Refs. 7 and 15–17), at which the expansion of the insect beyond its initial hosts is unpreventable and localization of the affected areas is technically impractical. Consequently, a large amount of resources has been devoted to utilizing remote sensing data to detect and map infested areas at the GA stage, in hope of improving the efficacy of treatment practices. However, the applicability of remote sensing observations (both space- and airborne) for GA detection and mapping has been argued to be practically impossible due to several biological (e.g., the timing of specific phenomena related to the infestation and movement) and technological (i.e., spatial, temporal, and spectral resolution requirements) limitations (please refer to Refs. 7 and 18 for a detailed review).

As previously stated, one of the earliest signs of the infestation is a drop in the sapwood moisture as a result of the introduction of a blue-staining fungi carried by the beetles as they bore through the bark. The spores of fungi penetrate living cells in the phloem and xylem, resulting in disruption of water flow,[19] which causes the leaves to close their stomata as a first stress-induced physiological response of vegetation in order to preserve water.[13] This behavior leads to a decrease in transpiration cooling and therefore to an increase in leaf and canopy temperature.

The latter, in turn, leads to an increase in the emitted thermal infrared (TIR) radiation without visible changes to the green fraction of vegetation during the first weeks of attack. Although the land surface temperature (T_s) derived from the TIR portion of the electromagnetic spectrum is widely implemented in formulating the energy and water budgets at the surface-atmosphere interface and has been shown to be useful for monitoring plant–water relations (e.g., Refs. 20–22), its applicability to insect disturbance is yet to be explored.[23] The tight coupling between beetle activity, plant water status, and the thermal response allows us to assume that the increase in T_s over the areas affected by the mountain pine beetle as well as the differences between T_s of the infested areas and the areas that have not yet been affected could be employed for early detection of GA epicenters.

The second effect of stomatal closure is a change in the amount of liquid water in the canopy layer (e.g., Ref. 24) and consequent increase in the reflected short-wave infrared (SWIR) radiation.[25] Generally speaking, studies investigating the spectral detection of GA are sparse (and not up to date), usually focusing on the examination of pigment-driven spectral variations in the visible and near-infrared (NIR) regions (e.g., Refs. 26–30). Although declines in sapwood moisture content resulting from a beetle attack have been documented as early as the 1960s (e.g., Ref. 31), subsequent changes in leaf water content and in leaf spectral reflectance were carefully investigated only recently through observing the comparable water features in the NIR and SWIR regions in different datasets of infested trees.[32] Thus, we assume that the difference between stressed and unstressed vegetation could be emphasized even more by combining the TIR and SWIR response to the changes in canopy water status.

Based on the life cycle of beetles, the timing of the surveys must be coordinated relative to the appearance of attack symptoms in the tree-crown foliage. Generally speaking, the best way to show the advancing water stress is by means of change detection techniques that make use of image pairs: one for a preattack period and the other for a period immediately after the attack. Such a pair, however, could not always be available primarily due to weather conditions (i.e., cloudiness). If it is so, the single image could also be satisfactory to observe the infested areas if it is taken shortly after the infestation and has a reasonable spatial resolution relative to the size of affected patches. Our objective is, therefore, to use single spaceborne Landsat ETM+ imagery a. to test the applicability of thermal infrared imagery for detection of the mountain pine beetle attack at its early stage and b. to evaluate whether the incorporation of thermal and shortwave infrared spectral responses will improve the ability to detect GA through the use of moderate spatial resolution remote sensing imagery. The proposed methodology reflects the desire to anticipate end-user needs and at the same time develop an approach based on simultaneous observations in thermal, near-, and shortwave infrared domains. This study is our first attempt to detect GA level MPB outbreaks, and the results need simultaneous ground survey data for further validation.

2 Materials and Methods

2.1 Study Site, Field Data, and Study Assumptions

For our purposes we used the single-scene approach utilizing satellite data from a Landsat ETM+ image (Path/Row: 50/23) acquired on August 2, 1999 with almost zero percent cloud cover. The specific area of interest has been chosen arbitrarily within the entire Landsat scene and is delineated in Entiako Provincial Park, North-East of lake Entiako in British Columbia (AOI, Fig. 1, an inset). This area is located within a larger extent of the affected areas in the province (east to the provincial boundary in the Rocky Mountains, and west to a line over the Coastal Mountains) and excludes habitats largely unsuitable for MPB outbreaks (i.e., Pacific maritime and boreal forests).

The mountain pine beetle reference data were provided by British Columbia Ministry of Forests and Range[33] collected as an aerial survey of the entire province that records areas of tree mortality, judged from red and/or gray crowns on 1:250,000 NTS topographic maps. The

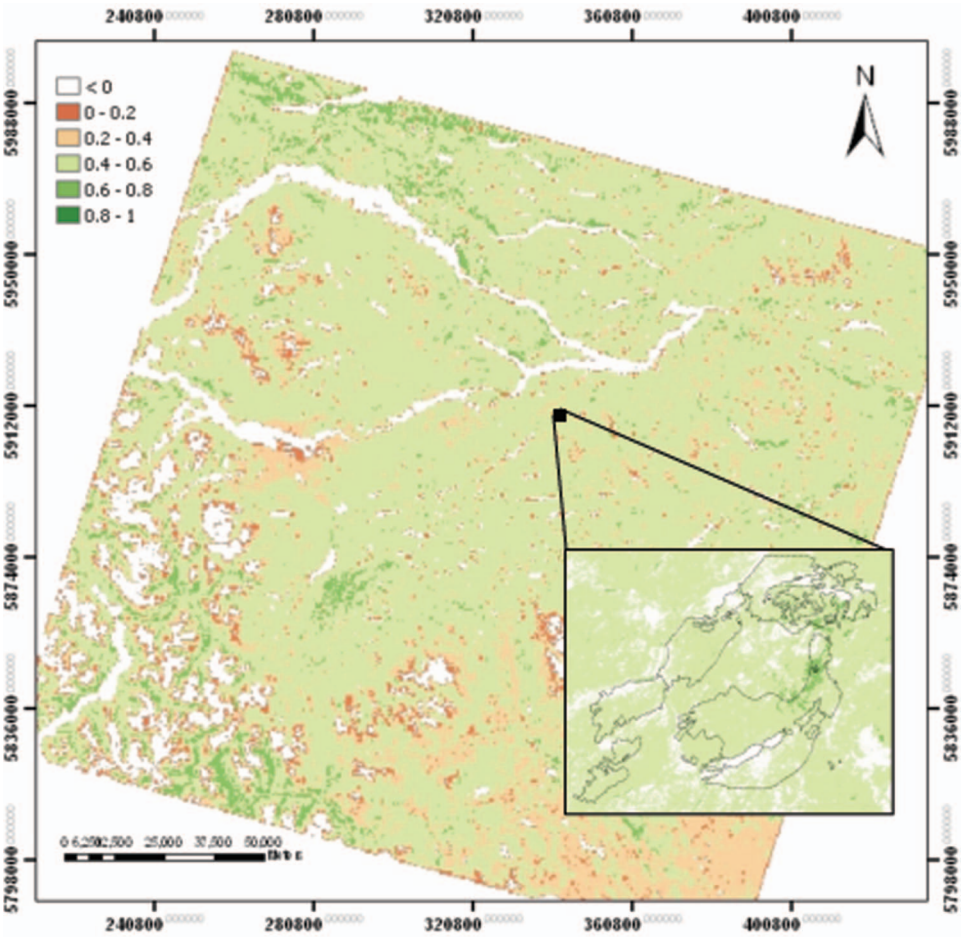

Fig. 1 NDVI map of the studied area. The specific area of interest is presented by an inset with a black line that indicates the boundary of a current RA area.

aerial survey data contains information on the spatial extent of all mortality inducing agents active in the province. For the purposes of this study only polygons delineating MPB affected areas were extracted. These polygons represent entire tree stands that contain both affected and unaffected trees and probably a mixture of red and green attacks. A severity classification based on the percentage of trees undergoing red attack within the stand is then assigned to each polygon (Table 1). It should be noted that since such a classification is heavily dependent on the subjective opinion of the surveyor, observation errors of infestation extent, such as inclusion of unsuitable habitat or overestimation of mortality due to the higher visual perceptibility of red foliage, are expected to occur at all severity classes.

Table 1 British Columbia Ministry of Forests and Range severity classification scheme.

Class number	Class name	Area infested (%)
1	Trace	<1
2	Light	1 to 10
3	Moderate	11 to 30
4	Severe	31 to 50
5	Very Severe	>50

The general assumption that we made regarding the aerial survey is that the area reported as RA in any year could be treated as GA in the preceding year.[34] Though this assumption relied on beetle phenology, the major drawback of such generalization is that reported RA areas are much larger than one could expect from GA, which is usually represented by several initially attacked trees. In other words, in every polygon reported as RA, the epicenter of increased temperature (as compared to adjacent areas) should be found, localized, and classified as GA in the preceding year.

The second assumption is that the GA areas (i.e., the areas that include the next generation of MPB) can usually be found in close vicinity to the areas classified as RA in the same year as beetles move gradually through the space.[7] The areas survey polygon data was overlaid onto the Landsat imagery in order to extract areas attributed to a certain severity class.

2.2 Image Processing and Moisture Condition Index Formulation

The Landsat scene was processed to retrieve a. surface reflectance in SWIR (band 5) and NIR (band 4) spectral domains and b. T_s from the thermal band data using the equations provided by the National Aeronautics and Space Administration (NASA;[35,36] http://landsathandbook.gsfc.nasa.gov/handbook.html) and a monowindow algorithm.[37] The thermal image was linearly resampled to 30 m resolution using ERDAS Imagine software in order to match the spatial resolution of NIR and SWIR bands.

Recognizing that surface temperature provides useful information about vegetation moisture conditions,[38] we formulated a temperature condition index (TCI) as:

$$\mathrm{TCI} = \frac{\mathrm{BT}_{\max} - \mathrm{BT}}{\mathrm{BT}_{\max} - \mathrm{BT}_{\min}}, \tag{1}$$

where BT, $\mathrm{BT}_{\min}$, and $\mathrm{BT}_{\max}$ are measured, averaged for a composite period or multiyear absolute minimum and maximum brightness (i.e., at-sensor) temperatures, respectively. We incorporated T_s (instead of BT) to Eq. (1) using "hot" and "cold" pixels as a proxy for extreme temperatures.[39] To do that BT has been converted to T_s by means of Plank's equation:

$$T_s = \frac{\mathrm{BT}}{1 + \left(\frac{\lambda \mathrm{BT}}{\rho}\right)} \ln\varepsilon, \tag{2}$$

where λ wavelength of emitted radiance ($=11.5\ \mu$m); $\rho = hc/\sigma$ with $\sigma = 1.38 \times 10^{-23}$ J/K), h $= 6.626 \times 10^{-34}$ Js, c $= 2.998 \times 10^{8}$ m/s and $\varepsilon = 0.98$ for vegetation.

As suggested earlier, the disruption of water flow induced by MPB's inoculation into the tree phloem will influence canopy reflectance in the SWIR domain. As the latter is also confounded by leaf and canopy properties[40] and it is sensitive to solar and sensor viewing geometry,[41] radiative transfer simulations at both leaf and canopy level[42–46] indicated that the ratio between NIR and SWIR reflectances could minimize the effect of these parameters.

We thus introduce the Moisture Condition Index (MCI) formulated as follows:

$$\mathrm{MCI} = \mathrm{TCI}\left(\frac{\mathrm{NIR}}{\mathrm{SWIR}}\right). \tag{3}$$

As formulated, both TCI and MCI decrease with T_s, being lower for stressed vegetation.

The reason for focusing on 1999 is that in earlier years the infestation had limited spatial extent so the attacked areas might be completely dissolved in moderate-resolution spaceborne TIR imagery, while in any year subsequent to 1999 the infestation in BC (as reported) was already widespread and different stages of the attack could co-exist within one pixel requiring implementation of more sophisticated within-pixel unmixing procedures, along with detailed field survey.

It must be noted that both the above-mentioned indices could be derived from any single image; such an approach would usually be complicated by natural surface variability other than the insect attack. This variability caused by topography, land cover, and land use variations (e.g., high surface temperature clear-cuts or low surface temperature snow-covered areas), has an influence on extreme values of surface temperature and thus on calculated indices widely stretching their range and blurring the real picture of infestation. Identifying and excluding these variations by means of change detection techniques is an important step in using TCI or MCI for insect detection. We found that the earliest available cloud-free Landsat scene of a preattack period covering the study area (see Sec. 2.1) was from September 1995. As T_s in September is expected to be naturally lower and thus incompatible to that in August, neither TCI nor MCI were calculated for 1995, and T_s-differences between two dates were used only to detect ground elements that can greatly stretch the T_s range. Since we do not have enough information about what these elements are and what are the reasons for a specific change in land-cover, we excluded them from further examination by filtering out pixels where the Normalized Difference Vegetation Index (NDVI) is lower than 0.4 (Fig. 1). We assume that these pixels represent either unforested areas or advanced phases of beetle attack (either red or gray attacks).[47,48] Providing the empirical nature of the comparison between the ground features at two different dates, the actual physical meaning of the pixel value was not crucial and the normalization between images has been deemed unnecessary in this particular case.[47]

2.3 Statistical Analysis

The severity classification scheme employed by BC's Ministry of Forests and Range has a large uncertainty (i.e., wide range of the percentage of affected areas) primarily because it is based on visual evaluation of the severity of infestation and manual sketching of infected stands. In such a way, the Ministry does not report within-polygon percentage of severity remaining only with a large-scale overall classification scheme as specified by Table 1. The main disadvantage of such an approximation is the allowance of almost arbitrary interpretation of the results.

Statistical analysis of the results has been performed by proportioning the number of pixels attributed to a highest MCI values ($2 \leq \mathrm{MCI} \leq 4$) within a certain polygon to the total number of pixels that belong to that polygon assuming that in an ideal case the pixels with the same MCI value will be equal to the total. We decided to refer only to severity classes 3 and 4, assuming that those classes of both MCI's and Ministry's (i.e., the only data available for validation) classifications represent the most distinct phases of an infestation detectable at the specific spatial resolution.

In an attempt to evaluate the quality of the results in the most appropriate and quantitative way that is possible under the current circumstances, we separated the range of values of each studied severity class (Table 1) into 5% subclasses (for instance, Class 3 has been separated into 11% to 15%; 15% to 20%; 20% to 25%, and 25% to 30% of severity). Finally, an error per subclass (ε) has been calculated as a relative difference between the total number of pixels in i-subclass (N_i) and the number of pixels with $2 \leq \mathrm{MCI} \leq 4$ (n):

$$\varepsilon = 100\left(\frac{N_i - n}{N_i}\right). \tag{4}$$

It should be noted that due to the way the severity classes are defined, the calculated errors are expected to be highly dispersed around a mean value. We also expect them to be higher for low severity classes (as they can be hardly detectable from the aircraft) decreasing with increasing severity of infestation (i.e., increase in infested area).

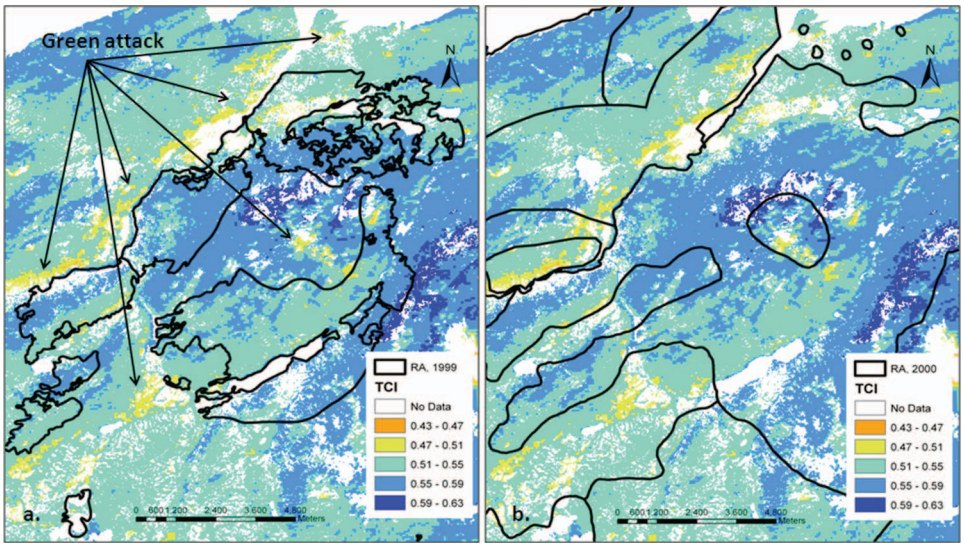

Fig. 2 The distribution of TCI over the specific area of interest. (a) RA areas as they were reported in the annual survey of the year 1999 are boarded by a black line. (b) GA areas (i.e., the areas that were reported as red attacked in the annual survey of the year 2000) are boarded by a black line.

3 Results and Discussion

3.1 Temperature Condition Index

Figure 2(a) shows the distribution of TCI over the specific AOI, indicating that the majority of the areas that were classified as RA (bordered by black line) have lower TCI (i.e., higher T_s) than their surroundings (average of ~0.53 as compared to ~0.58, respectively). Further analysis of the area in Fig. 2(a) reveals several hotspots of lower TCI (~0.48 on average) that appear within each RA boundary, presumably representing the epicenters of an outbreak. Figure 2(a) further shows that similar hotspots could be found at the adjacent areas (as indicated by arrows) representing the extension of the attack and the stands that include the next generation of the host trees. Those areas could be classified as GA areas in the current year and expected to be included in the next annual report (i.e., 2000). This last point is supported by Fig. 2(b) that presents the distribution of TCI overlapped by the results of the 2000 (black line) annual survey. The latter covers all the areas that were expected to be under GA in the preceding year. This is in agreement with our reasoning that GA areas are adjacent to RA areas as beetles move gradually through the landscape.

Another point that should be mentioned is the close similarity between TCI values of RA and GA hot spots as well as the small range of the values found ($0.45 < \text{TCI} < 0.55$). This similarity could be explained by the fact that once the water flow is disturbed and the tree closes its stomata to preserve water during the first weeks of attack, further changes in its temperature are only expected as part of the annual temperature oscillations. Consequently, the RA areas are not expected to have higher T_s than those that are under the GA. Furthermore, during the advanced stages of the attack, an increased canopy opening results in increased penetration of solar radiation to the forest floor, stimulating the growth of the secondary overstory and understory vegetation. The latter will lower T_s, causing an increase in the calculated index, potentially providing a reason for the close similarity between the values of both indices that have been observed for GA and RA. This similarity may be a limiting factor for using currently available spaceborne TIR observations as a stand-alone tool for detailed synoptic monitoring of the initial phases of mountain pine beetle infestation. This supports our initial assumptions that a combination of TIR with visible and/or near- and shortwave infrared (VNIR-SWIR)

observations is required for a successful separation between RA and GA areas. The above argument is correct if the area surveyed is already infested and includes patches of all three phases of the infestation.

It should also be noted that the lowest values of TCI that have been found in the specific Landsat scene (and consequently over the AOI; ~0.45) could not be always assigned to a "real" stress condition since, as emphasized by Refs. 34 and 43, stressed vegetation frequently have TCI < 0.3. The larger values found in our study with Landsat data may be due to the fact that insect-infected areas are generally patchy and smaller than the image resolution, so that some healthy trees are often mixed in the pixels. In consideration of the limitation of the image spatial resolution, the spatial variability in the index would certainly be more important than its exact range. A more detailed analysis involving ground measurements of sap flow in infected trees in conjunction with the high spatial resolution, airborne TIR and VNIR images acquisition would be useful to overcome this limitation and highly desirable for quantitative assessment of the insect damage in relation to TCI.

3.2 Moisture Condition Index

Figure 3 presents the distribution of MCI over the specific AOI overlapped with the boundaries of RA and GA areas [Figs. 3(a) and 3(b), respectively). As expected, inclusion of the SWIR reflectance band emphasizes the disparity between affected and unaffected areas in a sharper way than does TCI alone. It also shows that the difference between MCI's average values of the affected and the unaffected areas (3 and 5, respectively) is about 25% higher than their TCI-based counterparts (0.53 and 0.58, respectively). In addition, Fig. 3 demonstrates that the epicentres of a GA (dark-orange colored areas) in the current (i.e., 1999) year could be found and delineated in a more accurate and easier way with MCI than with TCI.

The quantitative comparison between observed and estimated datasets of each severity class separately [shown by colored polygons in Fig. 3(b)] shows a gradual decrease in calculated errors from ~81 ± 44% (± standard deviation) to ~14 ± 11% on average for higher and lower ends of sub-severity classification (11% to 30% for class 3 and 31% to 50% for class 4) following the increase in the area affected by MPB (i.e., the percentage of the severity; Table 2). Such

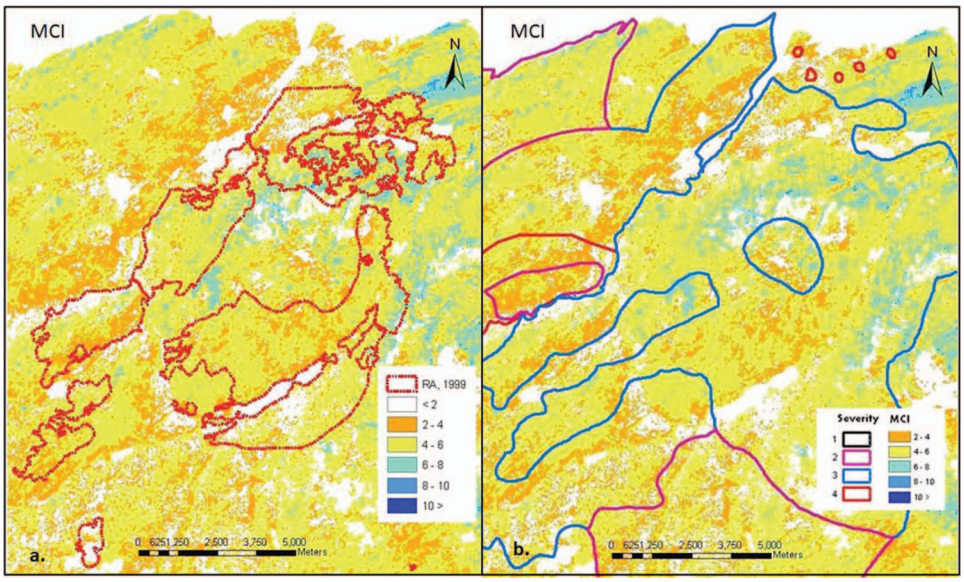

Fig. 3 The distribution of SWIR-corrected TCI over the specific area of interest overlapped by the boundaries of red and green areas [(a) and (b), respectively].

Table 2 Distribution of errors for British Columbia Ministry of Forests and Range severity classes 3 and 4 calculated per sub-severity class. All values are in percent.

Class 3		Class 4			
Area infested (%)	**Error**	**Area infested (%)**	**Error**	**Average error**	**STD**
11	81.20	31	50.37	81	44
15	55.59	35	33.19	44	16
20	16.69	40	16.54	17	0
25	6.64	45	3.59	5	2
30	22.20	50	6.77	14	11

an error distribution can be explained by the fact that the ability of the surveyor to distinguish between affected and unaffected areas increases with an increase in the infested area itself. On the other hand, the Landsat spatial resolution limits the sensitivity of MCI to low severity classes (and sub-classes) and is expected to increase with an increase in the area affected by insect.

Although all the results match our preliminary expectations, we are convinced that due to an uncertainty in the way the severity classes are defined and the lack of proper reference information, the overall performance of MCI could only be meaningfully evaluated by the error of either median or mean at each sub-class. This representative error is almost equal for both severity classes ($\sim$17.1 $\pm$ 0.6%) and fairly sufficient to conclude that the proposed index is an appropriate way to differentiate between different phases of the attack and under certain conditions could be used to detect the earliest stages of infestation. Figures 2 and 3 provide several other interesting spatial patterns with respect to the location of GA areas in relation to RA areas. First, GA areas are not always found in the immediate vicinity to RA [see, for example, the North-East corner of Fig. 2(b)]. This may be related to the fact that the mountain pine beetle does not attack every tree in the stand at its endemic state but only those that are of sufficient size,[49] although it is not completely understood how suitable trees are selected by bark beetles.[6] Second, the annual survey in 2000 does not include all the areas that are expected to be GA in the preceding year. We assume that at the time of the survey, those areas had not developed distinct visual signs and could possibly be missed by the surveyors. This fact, along with the similarity between T_s of GA and RA areas discussed earlier, is a limiting factor that could be overcome by simultaneous observations in TIR, SWIR, and VNIR domains.

4 Conclusions

A detection of the areas affected by the mountain pine beetle at the early stages of attack by means of remote sensing is of value to the monitoring and management of forests. Based on our understanding of the beetle-induced disruption of the sap-flow leading to a decrease in transpiration cooling and an increase in canopy temperature, we demonstrate that thermal infrared imagery could be useful for differentiating between infested and healthy vegetation. The TCI is used for this purpose. We further elaborate this issue by developing a new MCI, which is the TCI multiplied by the NIR to SWIR reflectance ratio, to account for the decrease in the amount of liquid water in the canopy as a second consequence of the insect attack. We show that MCI is more effective in detecting GA than TCI.

The current research is a first attempt to identify GA areas by means of thermal infrared imagery and an effort has been made to map the future extent of beetle infestation. Although the major uncertainty of our work comes from the lack of a proper field data as, to the best of our knowledge, such data does not exist over a large spatial scale, it is encouraging to note that areas reported as GA by the MCI index closely resemble the expected pattern of mountain pine beetle dispersal: beetles attack clusters of trees rather than entire areas. It is rare to encounter an area of forest that is completely infected by the beetle, especially on the leading edge of the outbreak. In this respect, further research should focus on a much smaller spatial scale (in

order of several hectares) where the beetle activity is well known and the mixture of RA and GA within a certain area could be validated by detailed field observations of actual green attack areas, and where proper and simultaneous measurements of water use (i.e., sap flow or water potential) could be carried out. The above-mentioned data collection, along with multispectral and thermal imagery, would serve to confirm the assumptions made in this study.

For the purposes of practicality, the prediction of GA areas using a combination of TIR and VNIR data can serve as a tool for mitigation purposes, such as directing harvest efforts to GA areas in order to prevent widespread dispersal from these areas in the following year, or as a tool to highlight areas to acquire higher spatial resolution imagery to be combined with aerial survey data for guiding finer scale surveys. At the same time, however, TIR imagery alone could be a useful tool for monitoring unmixed and unaffected areas since, all else being equal, the observed spatial differences in T_s (or any of its derivatives) is the first indicator of possible stress induced by the insect. Ground surveyors could then be guided to locations with the largest stress detected by remote sensing.

Such a strategy provides practical usefulness and is relatively cost effective when compared with aerial overview survey operations performed by British Columbia Ministry of Forests and Range. Since the outbreaks of the mountain pine beetle are very widespread, the management of the large affected area would necessitate a mosaic of a significant number of Landsat scenes, and the normalization of these images would be an additional step for large-area GA detection.

It should also be noted that the beetle naturally attacks trees that are already stressed, often at locations with low soil moisture levels. In these locations, the canopy temperature would generally be higher than the surroundings and could produce MCI values similar to those under GA. Such persistently stressed areas may be identified from a multiyear series of images. In this respect, the accuracy of the GA detection can be further improved.

References

1. K. F. Raffa, B. H. Aukema, B. J. Bentz, A. L. Carroll, J. A. Hicke, M. G. Turner, and W. H. Romme, "Cross-scale drivers of natural disturbances prone to anthropogenic amplification: The dynamics of bark beetle eruptions," *BioScience* **58**(6), 501–517 (2008).
2. J. A. Logan and J. A. Powell, "Ghost forests, global warming and the mountain pine beetle (Coleoptera: Scolytidae)," *Amer. Entom.* **47**(3), 160–172 (2001).
3. A. Walton, J. Hughes, M. Eng, A. Fall, T. Shore, B. Riel, and P. Hall, "Provincial-level projection of the current mountain pine beetle outbreak. Update of the infestation projection based on the 2007 provincial aerial overview of forest health and revisions to the "model" (BCMPB.v5)," available at http://www.for.gov.bc.ca/hre/bcmpb/BCMPB.v5.BeetleProjection.Update.pdf.
4. S. W. Taylor, A. L. Carroll, R. I. Alfaro, and L. Safranyik, in *The Mountain Pine Beetle: A Synthesis of Biology, Management and Impacts in Lodgepole Pine*, L. Safranyik and B. Wilson, Eds., Natural Resources Canada, Canadian Forest Service, Victoria (2006).
5. D. W. Williams and A. M. Liebhold, "Climate change and the outbreak ranges of two North American bark beetles," *Agric. For. Entomol.* **4**, 87–99 (2002).
6. K. O. Niemann and F. Visintini, "Assessment of potential for remote sensing detection of bark beetle-infested areas during green attack: A literature review," *Mountain Pine Beetle Initiative Working Paper 2005–2*, Natural Resources Canada Canadian Forest Service, Victoria (2004).
7. M. A. Wulder, C. C. Dymond, J. C. White, D. J. Leckie, and A. L. Carroll, "Surveying mountain pine beetle damage of forests: A review of remote sensing opportunities," *For. Ecol. Manag.* **221**, 27–41 (2006).
8. M. A. Wulder, J. C. White, A. L. Carroll, and N. C. Coops, "Challenges for the operational detection of mountain pine beetle green attack with remote sensing," *For. Chronicle* **85** (1), 32–38 (2009).
9. L. Safranyik, and A. L. Carroll, "The biology and epidemiology of the mountain pine

beetle in lodgepole pine forests," in *The Mountain Pine Beetle: a Synthesis of its Biology, Management and Impacts on Lodgepole Pine*, pp. 3–66, L. Safranyik and B. Wilson, Eds., Natural Resources Canada, Canadian Forest Service, Pacific Forestry Centre, Victoria, British Columbia (2006).

10. A. L. Carroll, S. W. Taylor, J. Régnière, and L. Safranyik, "Effects of climate change on range expansion by the mountain pine beetle in British Columbia," in *Proc. Mountain pine beetle symp.: Challenges and solutions*, pp. 223–232, B. C. T. L. Shore, J. E. Brooks, and J. E. Stone, Eds., Natural Resources Canada, Canadian Forest Service, Pacific Forestry Centre, Victoria, British Columbia, Information Report BCX- 399 (2004).
11. L. Unger, "Mountain pine beetle," *Forest Pest Leaflet*, Forestry Canada, Forest Insect and Desease Survey, Pacific Forestry Center, Victoria, British Columbia, Canada (1993).
12. M. A. Wulder and C. C. Dymond, "Remote sensing technologies For mountain pine beetle surveys," in *Proc. Mountain pine beetle symp.: Challenges and solutions*, T. L. Shore, J. E. Brooks, and J. E. Stone, Eds., Natural Resources Canada, Canadian Forest Service, Pacific Forestry Centre, Information Report BC-X-399, Victoria, British Columbia, 298 p (2004).
13. Y. Yamaoka, R. H. Swanson, and Y. Hiratsuka, "Inoculation of lodgepole pine with four blue-stain fungi associated with mountain pine beetle, monitored by a heat pulse velocity (HPV) instrument," *Can. J. For. Res.* **20**, 31–36 (1990).
14. L. Safranyik and C. Vithayasai, "Some charactristics of the spatial arrangement of attacks by the Mountain Pine Beetle, *Dendroctonus Ponderosae* (Coleoptera: Scolytidae), on lodgepole pine," *Can. Entomol.* **103**, 1607–1625 (1971).
15. S. Franklin, M. Wulder, R. Skakun, and A. Carroll, "Mountain pine beetle red-attack damage classification using stratified Landsat TM data in British Columbia, Canada," *Photogramm. Eng. Remote Sens.* **69**, 283–288 (2003).
16. J. C. White, M. A. Wulder, D. Brooks, R. Reich, and R. Wheate, "Mapping mountain pine beetle infestation with high spatial resolution satellite imagery," *Remote Sens. Environ.* **96**, 240–251 (2005).
17. N. C. Coops, M. Johnson, M. A. Wulder, and J. C. White, "Assessment of QuickBird high spatial resolution imagery to detect red-attack damage due to mountain pine beetle infestation," *Remote Sens. Environ.* **103**, 67–80 (2006).
18. M. A. Wulder, J. C. White, N. C. Coops, and C. R. Butson, "Multi-temporal analysis of high spatial resolution imagery for disturbance monitoring," *Remote Sens. Environ.* **112**, 2729–2740 (2008).
19. L. Safranyik, D. M. Shrimpton, and H. S. Whitney, "An interpretation of the interaction between lodgepole pine, the mountain pine beetle, and its associated blue stain fungi in western Canada," *Management of Lodgepole Pine Ecosystems*, pp. 406–428, D. M. Baumgartner, Ed., Washington State University Cooperative Extension Service, Pullman, Washington (1975).
20. S. B. Idso, R. J. Reginato, and R. D. Jackson, "An equation for potential evaporation from soil, water and crop surfaces adaptable to use by remote sensing," *Geophys. Res. Lett.* **4**, 187–188, (1978).
21. R. D. Jackson, J. L. Hatfield, R. J. Reginato, S. B. Idso, and P. J. Pinter, "Estimation of daily evapotranspiration from one time-of-day measurements," *Agric. Water Manage.* **7**, 351–362 (1983).
22. M. S. Moran, T. R. Clarke, Y. Inoue, and A. Vidal, "Estimating crop water-deficit using the relation between surface-air temperature and spectral vegetation index," *Remote Sens. Environ.* **49**, 246–263 (1994).
23. M. Heis and T. Kucera, "Surface temperature change of spruce forest as a result of bark beetle attack: Remote sensing and GIS approach," *Europ. J. For. Res.* **127**, 327–336 (2004).
24. K. Gibson and J. F. Negron, "Fire and bark beetle interactions," in *The Western Bark Beetle Research Group: A Unique Collaboration with Forest Health Protection*, J. L. Hayes and J. E. Lundquist, Eds., pp. 51–70, Proc. Symp. Soc. Amer. For. Gen. Tech. Rep.

PNW-GTR-784, U.S. Department of Agriculture, Forest Service, Pacific Northwest Research Station, Portland, Oregon (2009).
25. B. C. Gao, "NDWI a normalized difference water index for remote sensing of vegetation liquid water from space," *Remote Sens. Environ.* **58**, 257–266 (1996).
26. R. C. Heller, "Pre-visual detection of ponderosa pine trees dying from bark beetle attack," in *Proceedings of the 5th International Symposium Remote Sens. Environ.*, pp. 387–418 (1968).
27. G. S. Puritch, "Non-visual remote sensing of trees affected by stress: A review," Environment Canada, Canadian Forestry Service, Pacific Forest Research Centre, Victoria, British Columbia, *Information Report BC-X-30*, 38 pp. (1981).
28. P. Murtha and R. J. Wiart, "PC-based digital image analysis for mountain pine beetle green attack: Preliminary results," *Can. J. Remote Sens.* **13**, 92–95 (1987).
29. F. J. Ahern, "The effects of bark beetle stress on the foliar spectral reflectance of lodgepole pine," *Int. J. Remote Sens.* **9**, 1451–1468 (1988).
30. U. T. Runesson, "Considerations for early remote detection of mountain pine beetle in green-foliaged lodgepole pine," PhD Dissertation, University of British Columbia, Canada (1991).
31. R. W. Reid, "Moisture changes in lodgepole pine before and after attack by the mountain pine beetle," *For. Chronicle* **37**(4), 368–375 (1961).
32. T. Cheng, B. Rivard, G. A. Sánchez-Azofeifa, J. Feng, and M. Calvo-Polanco, "Continuous wavelet analysis for the detection of green attack damage due to mountain pine beetle infestation," *Remote Sens. Environ.* **114**, 899–910 (2010).
33. J. Westfall, "Summary of forest health conditions in British Columbia," *British Columbia Ministry of Forests and Range*, Forest Practices Branch, Victoria, British Columbia (2008).
34. R. G. Mitchell and H. K. Preisler, "Analysis of spatial patterns of lodgepole pine attacked by outbreak populations of the mountain pine beetle," *For. Sci.* **37**(5), 1390–1408 (1991).
35. B. L. Markham and J. L. Barker, "Landsat-MSS and TM post calibration dynamic ranges, atmospheric refectance and at-satellite temperature," EOSAT Landsat Technical Notes 1, Lanham, Maryland: Earth Observation Satellite Company, pp. 3–8 (1986).
36. K. Schneider and W. Mauser, "Processing and accuracy of Landsat ThematicMapper data for lake surface temperature measurement," *Int. J. Remote Sens.* **17**, 2027–2041 (1996).
37. Z. Qin, A. Karnieli, and P. Berliner, "A mono-window algorithm for retrieving land surface temperature from Landsat TM data and its application to the Israel-Egypt border region," *Int. J. Remote Sens.* **22**(18), 3719–3746 (2001).
38. F. N. Kogan, "Application of vegetation index and brightness temperature for drought detection," *Adv. Space Res.* **15**, 91–100 (1995).
39. W. G. M. Bastiaanssen, M. Menenti, R. A. Feddes, and A. A. M. Holtslag, "The surface energy balance algorithm for land (SEBAL): Part 1 formulation," *J. Hydrol.* **212–213**, 198–212 (1998).
40. P. Ceccato, N. Gobron, S. Flasse, B. Pinty, and S. Tarantola, "Designing a spectral index to estimate vegetation water content from remote sensing data: Part 1 Theoretical approach," *Remote Sens. Environ.* **82**, 188–197 (2001).
41. A. Ghulam, Z. L. Li, Q. Qin, Q. Tong, J. Wang, A. Kasimu, and L. Zhu, "A method for canopy water content estimation for highly vegetated surfaces–shortwave infrared perpendicular water stress index," *Sci. China Ser. D: Earth Sci.* **50**, 1359–1368 (2007).
42. P. Ceccato, S. Flasse, S. Tarantola, S. Jacquemound, and J. M. Gregorie, "Detecting vegetation leaf water content using reflectance in optical domain," *Remote Sen. Environ.* **77**, 22–33 (2001).
43. D. A. Sims and J. A. Gamon, "Estimation of vegetation water content and photosynthetic tissue area from spectral reflectance: A comparison of indices based on liquid water and chlorophyll absorption features," *Remote Sens. Environ.* **84**, 526–537 (2003).
44. F. M. Danson and P. Bowyer, "Estimating live fuel moisture content from remotely sensed reflectance," *Remote Sens. Environ.* **92**, 309–321 (2004).

45. J. T. Morisette, F. Baret, J. L. Privette, R. B. Myneni, et.al, "Validation of global moderate-resolution LAI products: A framework proposed within the CEOS land product validation subgroup," *IEEE Trans. Geosci. Remote Sens.* **44**(7), 1804–1817 (2006).
46. Y. Gu, J. F. Brown, J. P. Verdin, and B. Wardlow, "A five-year analysis of MODIS NDVI and NDWI for grassland drought assessment over the central Great Plains of the United States," *Geoph. Res. Lett.* **34**, L06407 (2007).
47. D. Song, P. Guo, and H. Sheng, "Spatial distribution pattern of MODIS-NDVI and correlation between NDVI and meteorology factors in Shandong Province in China," *PIERS ONLINE* **4**(2), 191–196 (2008).
48. L. S. Unganai and F. Kogan, "Drought monitoring and corn yield estimation in Southern Africa from AVHRR data," *Remote Sens. Environ.* **63**, 219–232 (1998).
49. T. L. Shore and L. Safranyik, "Susceptibility and risk rating systems for the mountain pine beetle in lodgepole pine stands," Forestry Canada, Pacific and Yukon Region, Information Report BC-X-336 (1992).

Biographies and photographs of the authors not available.